

pubs.acs.org/synthbio Research Article

Recombination of 2Fe-2S Ferredoxins Reveals Differences in the Inheritance of Thermostability and Midpoint Potential

Ian J. Campbell, Dimithree Kahanda, Joshua T. Atkinson, Othneil Noble Sparks, Jinyoung Kim, Chia-Ping Tseng, Rafael Verduzco, George N. Bennett, and Jonathan J. Silberg*



Cite This: ACS Synth. Biol. 2020, 9, 3245-3253



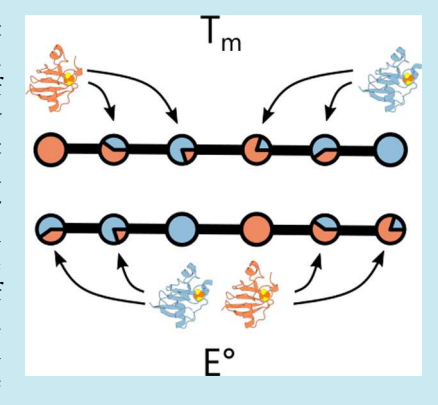
ACCESS

III Metrics & More



s Supporting Information

ABSTRACT: Recombination can be used in the laboratory to overcome component limitations in synthetic biology by creating enzymes that exhibit distinct activities and stabilities from native proteins. To investigate how recombination affects the properties of an oxidoreductase that transfers electrons in cells, we created ferredoxin (Fd) chimeras by recombining distantly related cyanobacterial and cyanomyophage Fds (53% identity) that present similar midpoint potentials but distinct thermostabilities. Fd chimeras having a wide range of amino acid substitutions retained the ability to coordinate an iron—sulfur cluster, although their thermostabilities varied with the fraction of residues inherited from each parent. The midpoint potentials of chimeric Fds also varied. However, all of the synthetic Fds exhibited midpoint potentials outside of the parental protein range. Each of the chimeric Fds could also support electron transfer between Fd-NADP reductase and sulfite reductase in *Escherichia coli*, although the chimeric Fds varied in the expression required for similar levels of cellular electron transfer. These results show how Fds can be diversified through recombination and reveal differences in the inheritance of thermo-



stability and electrochemical properties. Furthermore, they illustrate how electron transfer efficiencies of chimeric Fds can be rapidly evaluated using a synthetic metabolic pathway.

KEYWORDS: midpoint potential, electron transfer, recombination, ferredoxin, thermostability, sulfite reductase

erredoxins (Fds) are small soluble protein electron carriers that evolved to shuttle electrons in organisms across the tree of life, with some cells having genomes that encode as many as three dozen paralogs. 1 Fds transfer electrons between a wide range of partner oxidoreductases, ranging from proteins involved in light harvesting and nutrient assimilation to steroid synthesis and porphyrin metabolism.²⁻⁷ Among all protein electron carriers, Fds present some of the lowest midpoint reduction potentials (E°), with [2Fe-2S] Fds ranging from -150 to -500 mV and [4Fe-4S] Fds ranging from -200 to -650 mV.² While Fds are thought to control cellular electron transfer (ET) between their diverse partners by evolving sequences with distinct partner affinities and electrochemical properties, we cannot yet anticipate a priori how changes in Fd primary structure alter these biochemical and biophysical properties for synthetic biology applications.

Homologous recombination can be used in the laboratory to study how primary structure controls protein function and to overcome component limitations in synthetic biology. ^{8,9} This approach is appealing to use for protein design because amino acid substitutions created by recombination are less disruptive than those created randomly, since the sequence blocks being swapped have already been selected by evolution for compatibility within native structures. ¹⁰ Recombination has been applied to a variety of metalloproteins, such as

cytochromes P450, laccases, and hydrogenases. These studies have revealed that recombination can lead to innovations in metalloproteins, creating chimeras with distinct properties from the parent proteins being bred, including higher catalytic activity, distinct substrate specificity profiles, and altered stabilities. The second stabilities are specificated by the second stabilities are second stabilities.

Only a small number of studies have examined the effects of recombination on Fd electron carriers. These efforts have largely focused on recombining Fds that are encoded by the same genome and exhibit high sequence identity. Amino acid substitutions created by recombination have yielded Fd chimeras with a range of properties, including decreased stability, solubility, and ET efficiencies with partner proteins. ^{15–19} In a few cases, recombination has yielded Fds with electrochemical properties that differ from the parental proteins. ^{15,16} In these studies, Fds with distinct E° were recombined, and the E° of the resulting chimeras were within the range of values bounded by the parental proteins, with the

Received: June 8, 2020 Published: November 23, 2020





 E° values depending upon the relative degree of structural similarity to each parent. Similarly, it has been observed that chimeras frequently present thermostabilities that fall between the thermostabilities of the parents recombined. The extent to which this trend applies to Fd chimeras has not been explored.

Biophysical studies have shown that changes in the hydrogen bonding network surrounding the Fd iron—sulfur cluster can lead to E° changes. Because the number of hydrogen bonds disrupted by recombination is inversely correlated with parental protein sequence identity, we hypothesized that recombination of distantly related Fds would alter E° more dramatically than observed in prior studies. To test this idea, we created a set of Fd chimeras by recombining homologues from the cyanobacterium Mastigocladus laminosus Fd (ml-Fd1) and a cyanophage PSSM-2 (pssm2-Fd), which exhibit 53% sequence identity. These Fds were chosen because they have near-identical midpoint reduction potentials ($E^{\circ} = -344$ and -336 mV), while their melting temperatures $(T_{\rm m})$ differ by >40 °C $(T_{\rm m}=28$ and 76 °C). $^{23-25}$ In each chimera created, we examined iron—sulfur cluster coordination, E° , thermostability, and ET in a cellular pathway. Surprisingly, every chimera coordinated an iron-sulfur cluster and supported cellular ET. However, chimeras presented varying stabilities, and many chimeras presented E° that were outside of the parental range.

RESULTS AND DISCUSSION

Chimera Design. ml-Fd1 and pssm2-Fd were targeted for design because they exhibit similar structures (RMSD = 0.4 Å) but differ in sequence (53% identity) at almost half of their positions (Figure 1). Many of the native sites that differ in

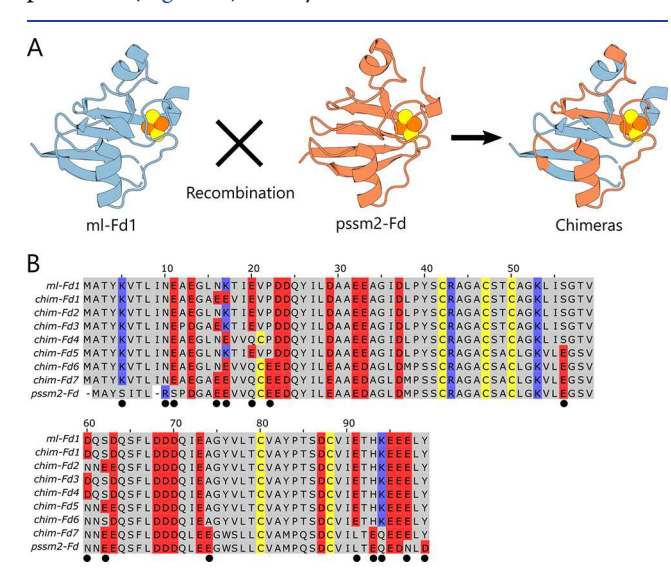


Figure 1. Comparison of parental and chimeric Fds. (A) Structures of ml-Fd1 (PDB: 1RFK) and pssm2-Fd (PDB: 6VJV), which were recombined to create chimeric Fds.^{24–26} (B) Alignment of the chimeric Fds and the parental proteins, which exhibit 53% identity, reveals residues that vary in charge (black circles).

sequence also vary in charge (n = 16) and possess functional groups that can form hydrogen bonds (n = 8). Even with these differences, the parental proteins contain similar total numbers of hydrogen bonds, with ml-Fd1 having 123 hydrogen bonds and pssm2-Fd having 133 hydrogen bonds. Because of the differences in the distribution of residues within the primary

structures of each parent, recombination has the potential to disrupt up to 51 total residue—residue contacts, including contacts that participate in hydrogen bonds (n = 38) and salt bridges (n = 4), molecular interactions that regulate Fd electrochemical properties.

In total, we generated seven chimeric ferredoxins (chim-Fd) which are numbered based on their mutational distance from ml-Fd1 (Table 1; Figure S1). To maximize the likelihood of

Table 1. Physicochemical Properties of Fd Chimeras^a

Fd	m _{ml-Fd1}	pI	$ heta_{427} \ (\mu ext{M})$	E° (mV/ SHE)	$T_{\rm m}$ (°C)	C_{broken}
ml-Fd1	0	3.9	0.28	-344	72.4 ± 0.2	0
chim-Fd1	4	3.75	0.25	-354	57.4 ± 1.0	11
chim-Fd2	4	3.94	0.21	-330	66.5 + 0.1	5
chim-Fd3	4	3.86	0.30	-392	64.4 ± 0.3	11
chim-Fd4	5	3.79	0.23	-396	67.1 ± 0.9	17
chim-Fd5	10	3.91	0.28	-384	65.5 ± 0.6	13
chim-Fd6	20	3.81	0.27	-360	41.1 ± 2.0	29
chim-Fd7	34	3.54	0.08	-319	21.0 ± 0.5	23
pssm2-Fd	47	3.5	0.25	-336	28.7 ± 0.5	0

^aProperties include isoionic point (pI), mutational distance from ml-Fd1 (m_{ml-Fd1}), ratio of ellipticity at 427 nm to concentration (θ_{427}/μ M), midpoint reduction potential (E°), melting temperature ($T_{\rm m}$), and residue—residue contacts broken by recombination relative to most similar parent ($C_{\rm broken}$). Melting temperatures are reported as the average of three measurements $\pm 1\sigma$.

generating folded chimeras, we used thermostable ml-Fd1 ($T_{\rm m}$ = 76 °C) as the scaffold and introduced residues from pssm2-Fd by swapping contiguous peptides from this lower stability Fd $(T_m = 28 \, ^{\circ}\text{C})$. This approach was used because prior studies have shown that thermostable proteins are more tolerant to amino acid substitutions.^{27,28} Chimeras were designed to sample different numbers of amino acid substitutions at varying locations within the primary structure. A small set of chimeras was targeted to enable comprehensive in vitro characterization and allow for calibration of the disruptive nature of recombination. 13,29 Chimeras were created with a range of amino acid substitutions (4 to 34) relative to ml-Fd1. These chimeras exhibited small variation in their absolute numbers of charged residues such that they all maintained the characteristically low pI found in Fds. 30-32 However, the chimeras differed in the total number of disrupted residue-residue contacts (5 to 29), number of disrupted hydrogen bonds (5 to 23), and number of disrupted salt bridges (0 to 1).

Cofactor Content and Thermostability. All of the chimeric Fds were purified using a combination of ion exchange and size exclusion chromatography. Each recombinant Fd presented a brown color immediately following purification, consistent with the presence of a 2Fe-2S cluster, although the final yields of each protein varied by >35-fold, with chim-Fd4 yielding 94 mg/L and chim-Fd7 yielding only 2.5 mg/L. To investigate which chimeric Fds contain ironsulfur clusters, we measured their absorbance and circular dichroism (CD) spectra and compared them with spectra obtained using purified ml-Fd1 and pssm2-Fd. In all cases, the chim-Fds presented absorbance spectra with peaks (465, 420, and 330 nm) that are characteristic of [2Fe-2S]-bound Fds (Figure S2). 32-34 Additionally the chim-Fds had CD spectra with ellipticity maxima (427 and 360 nm) and minima (505 and 560 nm) consistent with native holoFds (Figure 2).

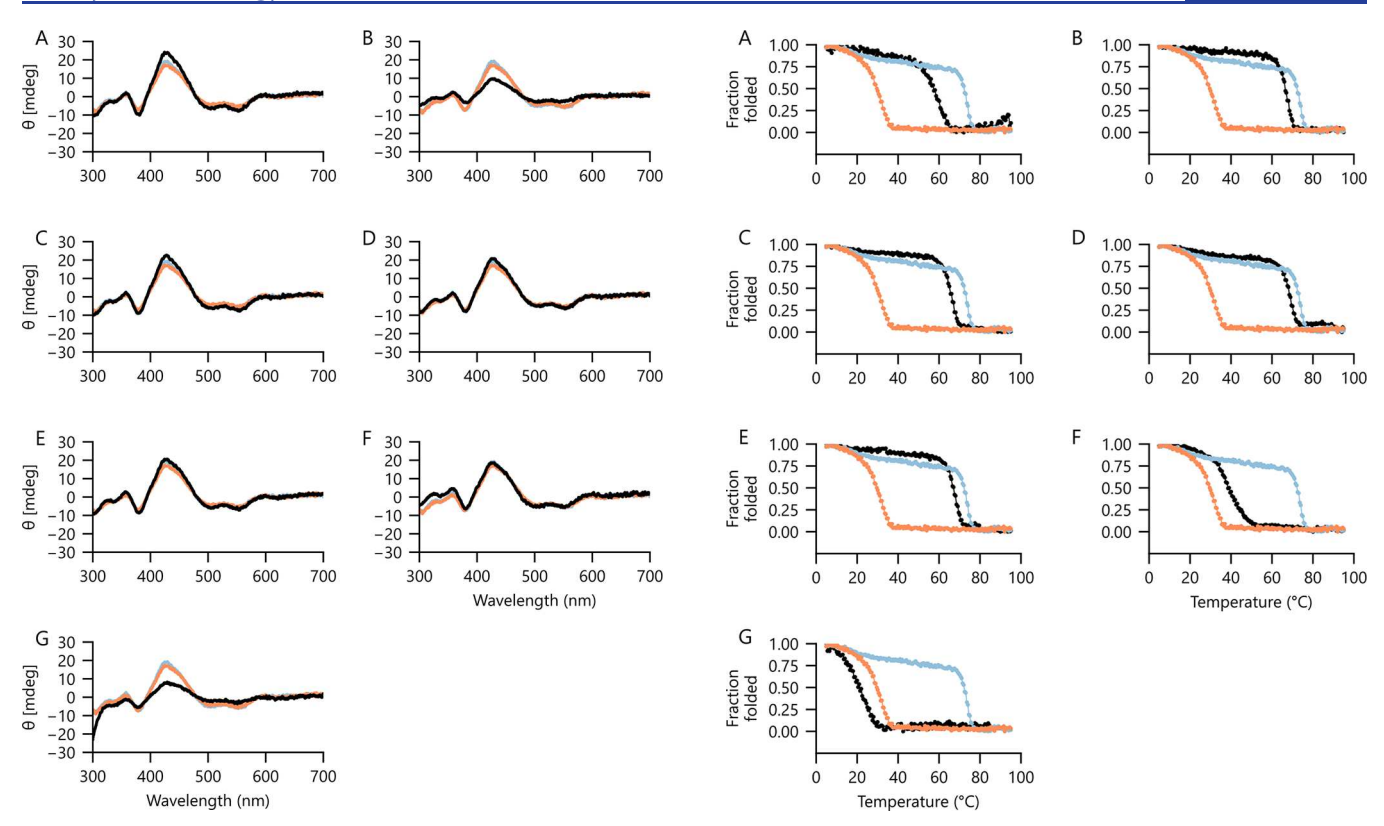


Figure 2. Circular dichroism spectra of chimeric Fds. The circular dichroism spectra of (A) chim-Fd1, (B) chim-Fd2, (C) chim-Fd3, (D) chim-Fd4, (E) chim-Fd5, (F) chim-Fd6, and (G) chim-Fd7 exhibit classic features of [2Fe-2S] Fds. Spectra for ml-Fd1 (blue) and pssm2-Fd (orange) are overlaid for comparison with each chimera (black). Measurements were performed using 50 μ M protein in TED buffer at 23 °C. For each protein, three independent measurements were performed, with a representative spectrum shown for each.

To compare chimera metallocluster content, we calculated the ratio of ellipticity at 427 nm to the concentrations determined using absorbance (Figure S3). While many of the chimeras presented ratios consistent with a high [2Fe-2S] occupancy (76–113% parental values), chim-Fd7 had a ratio corresponding to only 30% occupancy.

The thermostabilities of parental Fds differ by >40 °C, with pssm2-Fd and ml-Fd1 having $T_{\rm m}$ values of 28 and 76 °C, respectively. ^{24,25} To examine how the stabilities of the 2Fe-2S in the chim-Fds relate to the parental proteins, we measured how their ellipticities (427 nm) changed with increasing temperature (Figure 3). All of the chim-Fds exhibited temperature-dependent ellipticities. A majority of the chimeras exhibited midpoints for their loss of ellipticity at temperatures that are intermediate between the two parents, with the exception of chim-Fd7, which exhibited a lower midpoint value than pssm2-Fd. The five chimeras that are more closely related to ml-Fd1 (chim-Fd1, chim-Fd2, chim-Fd3, chim-Fd4, and chimFd-5) presented midpoint values in a narrow range (57 to 67 °C) while the other chimeras exhibited lower values (41 and 21 °C).

Electron Transfer in a Synthetic Pathway. The parental Fds can both support ET from Zea mays Fd-NADP reductase (FNR) to Zea mays sulfite reductase (SIR) within a synthetic cellular pathway. ^{23,24,35} In this pathway, ET is quantified by monitoring the growth of Escherichia coli EW11, a strain that cannot grow on medium containing sulfate as a sulfur source

Figure 3. Effect of temperature on iron—sulfur cluster coordination. The thermal denaturation of (A) chim-Fd1, (B) chim-Fd2, (C) chim-Fd3, (D) chim-Fd4, (E) chim-Fd5, (F) chim-Fd6, and (G) chim-Fd7 are shown in black. Melting curves for ml-Fd1 (blue) and pssm2-Fd (orange) are shown for comparison. All experiments were performed by monitoring ellipticity (427 nm) of samples containing 50 μ M protein in TED buffer at a scan rate of 1 °C/min. For each protein, three independent measurements were performed, with a representative spectrum shown for each.

unless it expresses a Fd that transfers electrons from FNR to SIR (Figures 4A).³⁵ When a Fd transfers electrons from FNR to SIR, sulfite is reduced to sulfide which can then be used for the synthesis of cysteine and methionine. To test whether any of the chimeras support ET from FNR to SIR, we electroporated E. coli EW11 with a plasmid that expresses each chimeric Fd using an anhydrotetracycline (aTc) inducible promoter and a plasmid that constitutively expresses FNR and SIR (Figure 4B). In all cases, cells expressing chimeric Fds showed significant growth following overnight incubations in the presence of aTc over the noninduced controls (Figure 4C). Five chimeras (chim-Fd2, -Fd3, -Fd4, -Fd5, and -Fd6) presented end point growth values that were similar to parental proteins. In contrast, the growth enhancement with chim-Fd1 and chim-Fd7 were both lower than parental proteins, even though these chim-Fds are the most closely related to the parental proteins.

Differences in chim-Fd expression could contribute to variation in ET from FNR to SIR and complementation of *E. coli* EW11 growth.²⁴ To test this idea, we fused each chim-Fd to red fluorescent protein (RFP) at its C-terminus using a (GSS)₄ linker and examined protein expression. In a prior study, we found that ml-Fd1 can be fused to RFP using this linker without affecting cellular ET.³⁶ With each Fd, whole cell fluorescence measurements normalized to OD₆₀₀ revealed a higher signal in the presence of aTc compared with uninduced

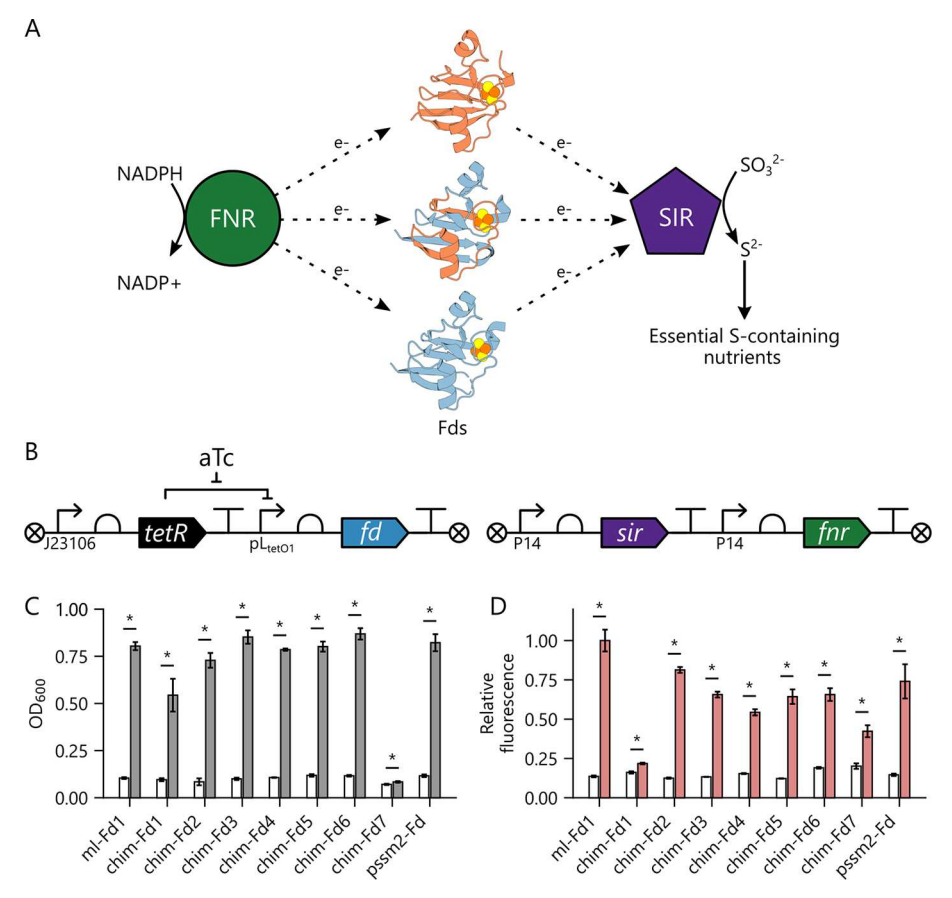
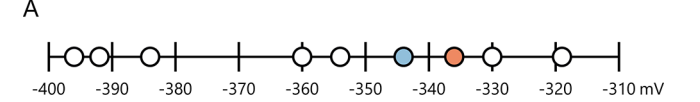


Figure 4. Chimeric Fds support ET between plant FNR and SIR. (A) The synthesis of essential sulfur-containing metabolites is dependent on Fd-mediated ET from FNR to SIR. (B) Genetic circuit used to express a synthetic ET pathway. Fds are expressed using an aTc-inducible promoter while constitutive promoters are used to express FNR and SIR. (C) Growth of *E. coli* EW11 in M9sa medium in the absence (white) and presence (gray) of aTc. Cells were cotransformed with a vector that constitutively expresses FNR and SIR and different vectors that express each Fd using an aTc-inducible promoter. (D) *E. coli* EW11 was transformed with vectors for expressing Fd-RFP fusions, and whole cell fluorescence was measured in uninduced (white) and induced (red) cells. Relative fluorescence represents emission divided by OD_{600} and normalized to the maximum value observed. All experiments were performed in triplicate, and an independent two-tailed *t* test was used to compare values \pm aTc (α = 0.05). Significant differences (p < 0.05) are noted with asterisks.

cultures (Figure 4D), with ml-Fd1-RFP presenting the largest aTc-dependent fluorescence. Most of the chim-Fds presented signals that were ≥50% of that observed with the parental Fds, with the exception of chim-Fd-1 and chim-Fd-7, which presented significantly lower signals. In some cases, the protein expression did not correlate with growth complementation. For example, chim-Fd7 presented the weakest growth complementation, but did not present the lowest expression.

Chimera Midpoint Reduction Potentials. Electrochemical changes arising from recombination could also contribute to the variation in E. coli EW11 complementation, since growth requires ET between partner proteins with defined midpoint potentials, FNR ($E^{\circ} = -337 \text{ mV}$) to SIR ($E^{\circ} = -285 \text{ mV}$). 37,38 To determine how the chim-Fd midpoint reduction potentials relate to those of the donor and acceptor proteins, we performed protein thin-film, square wave voltammetry on each chim-Fd (Figures S4-S5). Surprisingly, all of the chimeras presented E° outside of the range of the parental proteins (-344 to -336 mV) and all but two were more negative than the parents (Figure 5A). Several chimeras presented midpoint potentials lower than the most negative parent (ml-Fd1). The two chimeras presenting positively shifted E° from the parents had smaller shifts than those that were negatively shifted. These results can be contrasted with the T_{m} trends, which



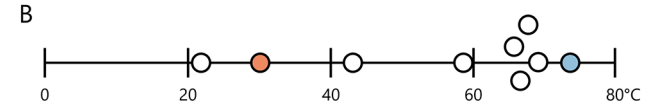


Figure 5. Midpoint potential and thermostability differ in inheritance patterns. (A) The E° of purified ml-Fd1 (blue) and pssm2-Fd (orange) are compared with the chim-Fds (white). E° were measured using square-wave thin-film protein voltammetry with concentrated protein samples (300 μ M) at pH 7 and 23.5 °C. (B) The $T_{\rm m}$ of chim-Fds (white) reveals values that are largely intermediate to ml-Fd1 (blue) and pssm2-Fd (orange). All thermostability measurements were performed by monitoring ellipticity (427 nm) of samples containing 50 μ M protein in TED buffer at a scan rate of 1 °C/min.

yielded chimera values bounded by the parental values (Figure 5B). While chim-Fds presented E° and $T_{\rm m}$ values that both differed from the parental Fds (Figure S6), these properties did not display a significant correlation (r=-0.56, p>0.1). A few of the chimeras (chim-Fd1 and chim-Fd2) presented small peaks near -150 mV (Figure S5B,C). The source of these

peaks is unknown but these signals may have arisen from dimerization of Fds, which has been observed in natural homologues. Dimerization could alter the local redox environment of the iron—sulfur cluster in some chim-Fds, shifting a small portion toward a more positive redox potential. Alternatively, it could arise from a small contaminant in our protein preparations or a degradation product of our protein following concentration for this measurement.

Biophysical Comparisons. To better understand the effects of recombination on protein thermostability, we compared the $T_{\rm m}$ values of each chimeric Fd with a range of physicochemical properties. A comparison of $T_{\rm m}$ with the calculated isoionic point (pI) revealed a significant correlation (r = 0.89, p < 0.005) (Figure 6A), as well as between pI and

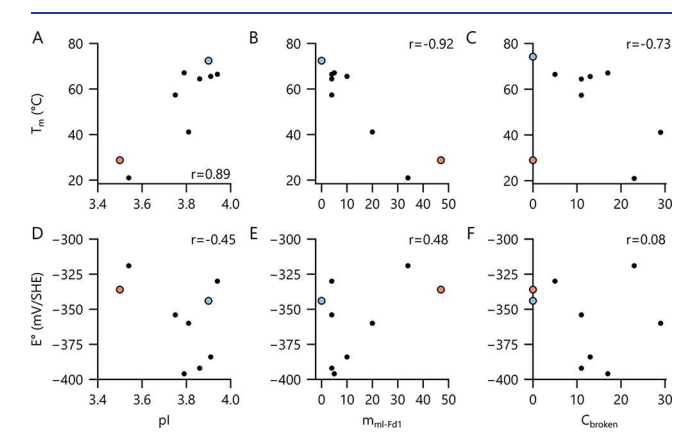


Figure 6. Biophysical correlations. The $T_{\rm m}$ values of Fds are compared to (A) calculated pI values, (B) mutational distance from the more thermostable ml-Fd1, $m_{\rm ml-Fd1}$, and (C) residue—residue contacts broken by recombination, $C_{\rm broken}$. The E° of each Fd is compared to (D) pI, (E) $m_{\rm ml-Fd1}$, and (F) $C_{\rm broken}$. Values from ml-Fd1 and pssm2-Fd are shown in blue and orange, respectively. Pearson correlations are shown in each panel. Significant correlations were observed between $T_{\rm m}$ and pI (p < 0.005) and $T_{\rm m}$ and mml-Fd1 (p < 0.0005). All other trends presented p values >0.05.

the absolute counts of charged amino acids in each chim-Fd (Figures S7A-C). These findings support the idea that electrostatics play a role in controlling the stabilities of Fds. 26,40,41 A comparison of $T_{\rm m}$ with mutational distance from ml-Fd1 (Figure 6B) yielded an even stronger correlation (r =-0.92, p < 0.005). Since some mutations disrupt structure by breaking residue-residue contacts critical to folding and function, we also evaluated whether the number of residueresidue contacts broken (C_{broken}) through recombination correlates with $T_{\rm m}$. This analysis showed that chim-Fds tolerate up to 20 broken residue-residue contacts before losses in T_m are observed (Figure 6C). We next evaluated whether the E° of the chim-Fds display any biophysical correlations. When similar comparisons were performed, weaker correlations were observed (Figures 6D-F; S7D-F), none of which were significant.

Implications for Oxidoreductase Design. Our results provide evidence that chim-Fds created by recombining distantly related parents (53% identity) display a high tolerance to amino acid substitutions. All of the chim-Fds characterized herein retained the ability to coordinate an iron–sulfur cluster, and they all supported ET from FNR to SIR in a synthetic cellular pathway, even though they presented a wide range of amino acid substitutions (4 to 34) and contacts

disrupted by recombination (5 to 29). These findings are similar to those obtained in a study examining the folding and function of chimeric cytochromes P450, which found that a vast majority of the chimeras having ≤35 amino acid substitutions and <35 disrupted residue-residue contacts retained the ability to fold, bind a metallocofactor, and perform catalysis.¹³ In contrast, a prior study examining the cellular function of lactamase chimeras created by recombining parents with 40% identity found that only a subset of the chimeras with ≤35 disrupted residue—residue contacts retained function. 42,43 Additionally, chimeric cellulases created by recombining distantly related parents (64% identity) exhibited a greater sensitivity to disrupted residue-residue contacts.²⁷ Cellulase chimeras having ≥15 broken residue-residue contacts were largely inactive. The underlying cause of these differences in the relationship between calculated and observed structural disruption is not known. They could arise because of variation in the number of parents recombined, similarity between parents, the number of crossovers used to generate chimeras, or parent stability. Additionally, these differences could be affected by the presence of metallocofactors in some of these proteins, which may confer additional stability and tolerance to amino acid substitutions arising from recombination.44-

In prior studies that have used recombination for protein design, the melting temperatures of the resulting chimeras has been found to correlate with the polypeptide inheritance from parental proteins. When three cytochromes P450 were recombined with distinct melting temperatures, the distribution of chimera thermostabilities could be predicted from the additive contributions of the sequence fragments inherited. 12,47 A vast majority of the chimeras presented melting temperatures that were intermediate to those of the parents, and chimeras only rarely exhibited higher or lower melting temperature values. Our results with chimeric Fds are consistent with these observations. Almost all of the chim-Fds exhibit melting temperatures that are intermediate to the parental proteins recombined. In contrast, the electrochemical properties of the chimeric Fds are all outside the range of the parental proteins. This trend is distinct from that observed in prior Fd recombination studies, which found that the E° of chimeras were bounded by the values of the parental proteins. 15,16 The underlying cause of the contrasting trend observed herein is not known. The two Fd chimeras with the largest midpoint reduction potential shifts arise from sequence changes on the β -strand most distal to the [2Fe-2S] cluster, although each chimera arises from amino acid substitutions on opposite ends of the strand. Additionally, chim-Fd5, which also presented a low E° , has sequence changes adjacent to a clusterligating cysteine.

Our results provide a calibration for calculated structural disruption estimated using the Schema algorithm. 48 Prior studies have found that as calculated disruption increases, the likelihood of protein folding and function decreases within different protein families. 42 We found that chimeras created using distantly related Fds retain the ability to support cellular ET ability in cases where calculated disruption is <30. This finding suggests that future chimeric libraries of Fds can be enriched in folded proteins by generating chimeras below this disruption threshold. By selecting large libraries of chim-Fds for variants that support ET between FNR and SIR, one could rapidly identify variants that are most efficient in this cellular pathway, since growth depends on Fd-mediated ET. Additionally, by varying FNR and SIR partners in this selection, which

may favor ET with distinct chimeras, selections could provide insight into the ways that Fd ET efficiencies in cells depend upon the structure of their partner proteins. Finally, by analyzing how the physical properties of chim-Fds vary with primary structure and cellular function, it may be possible to begin developing design rules that guide the creation of Fds with user specified thermostabilities, midpoint potentials, and cellular ET.

METHODS AND MATERIALS

Materials. Tris Base was from Fisher Scientific, *N*-cyclohexyl-3-aminopropanesulfonic (CAPS) was from Acros Organics, and 2-(*N*-Morpholino)ethanesulfonic acid (MES) and *N*-[Tris(hydroxymethyl)methyl]-3-aminopropanesulfonic acid (TAPS) were from Fluka Biochemika. Isopropyl β-D-1-thiogalactopyranoside (IPTG), dithiothreitol (DTT), kanamycin, chloramphenicol, and streptomycin were from Research Product International. 3-Morpholinopropane-1-sulfonic acid (MOPS), *N*-Cyclohexyl-2-aminoethanesulfonic acid (CHES), and all other chemicals were purchased from Sigma-Aldrich. *E. coli* EW11 was a gift from Pam Silver (Harvard University), 35 *E. coli* XL1-Blue was from Agilent, and *E. coli* Rosetta(DE3) was from Novagen.

Vector Design. All plasmids used for cellular measurements are listed in Table S1, while those used to overexpress proteins for purification are in Table S2. Native genes were synthesized by Integrated DNA technologies as G-blocks, and plasmids that express each chimeric protein were constructed by cloning these synthesized genes into pFd007 using Golden Gate DNA assembly. Plasmids were constructed by ligating PCR products amplified with Q5 High-Fidelity DNA polymerase (New England Biolabs) using Golden Gate DNA assembly. Ribosome binding sites were designed using the RBS calculator. All Fds had the same translation initiation site, except for pssm2-Fd. All plasmids were sequence verified.

Calculations. Alignments were made using MUSCLE and visualized using JalView. ^{51,52} pI values were estimated using ExPASy. ⁵³ Residue—residue contacts broken by recombination was calculated using SCHEMA. ⁹ Disruption of all chimeras was calculated relative to ml-Fd1 and is reported as a disruption score (C_{broken}). Pairwise amino acids were only counted if residues, including both side chain and main chain atoms, were within 4.5 Å of each other and recombination caused a change in sequence relative to parents. Hydrogen bonds and salt bridges were identified using PyMol. ⁵⁴

Protein Purification. E. coli Rosetta(DE3) transformed with pET28b-derived vectors containing Fds were grown at 37 °C in lysogeny broth (LB) containing 50 µg/mL kanamycin to exponential phase, induced at mid log phase using 50 μ M IPTG, and grown overnight at 37 °C while shaking at 250 rpm. Cells harvested by centrifugation (4000g) were resuspended in lysis buffer, which contained 10 mM Tris pH 8, 5 mM dithiothreitol (DTT), 10 mg/L DNase I, and 0.5 mg/mL lysozyme. After freezing at -80 °C, cells were thawed and mixed with cOmplete Mini, EDTA-Free protease inhibitor (Sigma-Aldrich) at a ratio of one tablet per 100 mL lysate. Clarified lysate harvested by centrifugation was diluted 3-fold with TED buffer (25 mM Tris pH 8, 1 mM EDTA, 1 mM DTT) and loaded onto a DE52 anion exchange column (Whatman). The column was washed with TED containing 200 mM NaCl, and the Fd was eluted using sequential isocratic washes with TED containing 250 and 300 mM NaCl. Fractions appearing brown were mixed, diluted with TED, and loaded

onto HiTrap Q XL column (GE Healthcare) using an AKTA Start FPLC system (GE Healthcare). After washing the column with TED, the protein was eluted using a linear gradient (0 to 375 mM NaCl in TED) followed by an isocratic wash (500 mM NaCl in TED). Brown fractions were pooled and then purified using a HiLoad 16/600 Superdex 75 (GE Healthcare) size exclusion column containing TED. SDS-PAGE was performed to analyze purity at each step using NuPage 12% Bis-Tris Gels (Invitrogen). Samples appearing homogeneous were pooled and concentrated using an Amicon Ultra 10 K MWCO spin column (EMD Millipore) and flash frozen with liquid nitrogen.

Spectroscopy. To obtain buffer matched controls, Fds were dialyzed into TED prior to all measurements. Absorbance spectra and ellipticity were acquired using a J-815 spectropolarimeter (Jasco, Inc.) using quartz cuvettes with a 1 cm path length. Scans were conducted using a 1 nm bandwidth, a 0.5 nm data pitch, and a 200 nm/min scan rate at 20 °C. To assess protein stability, a cuvette containing 50 μ M Fd was heated from 5 to 95 °C at a rate of 1 °C/min while monitoring ellipticity and absorbance. All spectra represent buffer corrected data.

Electrochemistry. Electrochemical measurements were performed anaerobically using a three-electrode system. A Ag/AgCl/1 M KCl electrode (CH Instruments) was used as the reference electrode, and a platinum wire was used as the counter electrode. Reference electrodes were regularly replenished with fresh KCl and calibrated using standards. An edge-plane pyrolytic graphite electrode was used as the working electrode to perform protein film electrochemistry. Prior to adding Fd, this electrode was treated with 100 mM neomycin trisulfate (Sigma-Aldrich) to improve the electrochemical signal.⁵⁵ An aliquot (3 μ L) of Fd (~300 μ M) was applied directly to the electrode surface following neomycin treatment, and the protein was allowed to adhere to the surface for 1 min at 23 °C. The electrode was then placed in a glass vial containing a pH 7 buffer solution (5 mM acetate, MES, MOPS, TAPS, CHES, CAPS) containing 100 mM NaCl at 23.5 °C. Square wave voltammograms were collected at 10 Hz frequency, and electrochemical signals were analyzed using Qsoas open software. Similar results were obtained when experiments were performed using pssm2-Fd from different purifications. In addition, the results for ml-Fd1 matched those obtained by our group and others in previous studies. 23,24,55 A CH Instruments potentiostat and CHI660E electrochemical analyzer were used for all measurements. All data are reported from single measurements and relative to Standard Hydrogen Electrode (SHE), taking into account the potential difference between SHE and Ag/AgCl/1 M KCl, which is 0.222 V. Differences in the ratios between protein concentration and current peak height were attributed to variation in insulating side chains among the different Fds analyzed.

Growth Assay. *E. coli* EW11 cells were transformed with two plasmids using electroporation, one constitutively expressing the electron donor and acceptor pair (FNR and SIR) and the other expressing a native Fd or a chimera as previously described. ^{23,35,36,56} To select for the Fd and partner plasmids, all growth steps included chloramphenicol (34 μ g/mL) and streptomycin (100 μ g/mL). Starter cultures were inoculated using single colonies. These starter cultures were grown in deep-well 96-well plates for 18 h at 37 °C in 1 mL of a nonselective modified M9 medium (M9c) as previously described. ²⁴ Starter cultures that had been grown to stationary

phase were centrifuged at 4 $^{\circ}$ C for 10 min at 3500g and resuspended in 1 mL of a selective modified M9 medium (M9sa), which is identical with M9c but lacks cysteine and methionine. Starter cultures were then diluted 1:100 into M9sa in Nunc Edge 2.0 96-well plates (Thermo Fisher). Cells were grown in the presence of the indicated amount of aTc in a Spark plate reader (Tecan) at 37 $^{\circ}$ C with shaking at 90 rpm at an amplitude of 3 mm in double-orbital mode. Optical density at 600 nm (OD₆₀₀) was measured for 48 h.

Cellular Fluorescence. These measurements were performed like the growth assay except cultures were grown in M9c throughout. After 48 h, OD_{600} and emission ($\lambda_{ex} = 560$ nm; $\lambda_{em} = 650$ nm) were measured. All values shown represent fluorescence normalized to OD_{600} .

Statistics. Error bars represent standard deviation calculated from three or more biological replicates. Independent, two-tailed t tests were used to compare differences between all relevant samples with $\alpha = 0.05$. All correlations shown are Pearson correlations calculated with NumPy.⁵⁷

ASSOCIATED CONTENT

Supporting Information

The Supporting Information is available free of charge at https://pubs.acs.org/doi/10.1021/acssynbio.0c00303.

List of vectors used for cellular assay in Table S1; List of vectors used for overexpression and purification in Table S2; Structural models of chimeric Fds in Figure S1; Absorbance spectra of chimeric Fds in Figure S2; Ironsulfur cluster content of chimeric Fds in Figure S3; Buffer-subtracted square wave voltammetry of chimeric Fds in Figure S4; Baseline square wave voltammetry of chimeric Fds in Figure S5; Comparison of chimera thermostability and midpoint potential in Figure S6; Comparisons of chimera amino acid composition, thermostability, and midpoint potential in Figure S7 (PDF)

AUTHOR INFORMATION

Corresponding Author

Jonathan J. Silberg — Department of BioSciences, Department of Chemical and Biomolecular Engineering, and Department of Bioengineering, Rice University, Houston, Texas 77005, United States; orcid.org/0000-0001-5612-0667; Phone: 713-348-3849; Email: joff@rice.edu

Authors

Ian J. Campbell – Department of BioSciences, Rice University, Houston, Texas 77005, United States; ⊙ orcid.org/0000-0003-3944-1260

Dimithree Kahanda — Department of BioSciences, Rice University, Houston, Texas 77005, United States; orcid.org/0000-0002-0009-7450

Joshua T. Atkinson – Department of BioSciences, Rice University, Houston, Texas 77005, United States; orcid.org/0000-0001-9293-4123

Othneil Noble Sparks — Department of BioSciences, Rice University, Houston, Texas 77005, United States;
orcid.org/0000-0002-4843-5009

Jinyoung Kim − Department of BioSciences, Rice University, Houston, Texas 77005, United States; o orcid.org/0000-0002-7107-3691 Chia-Ping Tseng — Department of Chemical and Biomolecular Engineering, Rice University, Houston, Texas 77005, United States; orcid.org/0000-0003-4124-4223

Rafael Verduzco — Department of Chemical and Biomolecular Engineering, Rice University, Houston, Texas 77005, United States; occid.org/0000-0002-3649-3455

George N. Bennett – Department of BioSciences and Department of Chemical and Biomolecular Engineering, Rice University, Houston, Texas 77005, United States; orcid.org/0000-0003-1408-8915

Complete contact information is available at: https://pubs.acs.org/10.1021/acssynbio.0c00303

Author Contributions

I.J.C., J.T.A., G.N.B., and J.J.S. conceptualized the project. I.J.C. designed chimeras. I.J.C. and J.K. built vectors. I.J.C. and O.N.S. purified protein. I.J.C. conducted spectroscopy. D.K., C.-P.T., I.J.C., and R.V. conducted electrochemistry. I.J.C. and J.K. conducted growth and fluorescence assays. I.J.C. and J.J.S. wrote the manuscript, and all other authors refined the text.

Notes

The authors declare no competing financial interest.

ACKNOWLEDGMENTS

This project was supported by DOE grant DE-SC0014462 (to J.J.S. and G.N.B.), NASA NAI grant 80NSSC18M0093 (to G.N.B. and J.J.S.), and NSF grant 1843556 (to G.N.B., J.J.S., and R.V.). I.J.C. and J.T.A. were supported by a Lodieska Stockbridge Vaughn Fellowship. C.P.T. is a participant in the NSF Research Traineeship 1828869 (to J.J.S., G.N.B., and R.V.).

■ REFERENCES

- (1) Campbell, I. J., Bennett, G. N., and Silberg, J. J. (2019) Evolutionary Relationships Between Low Potential Ferredoxin and Flavodoxin Electron Carriers. *Front. Energy Res.* 7, 79.
- (2) Atkinson, J. T., Campbell, I., Bennett, G. N., and Silberg, J. J. (2016) Cellular Assays for Ferredoxins: A Strategy for Understanding Electron Flow through Protein Carriers That Link Metabolic Pathways. *Biochemistry 55*, 7047–7064.
- (3) van den Heuvel, R. H. H., Svergun, D. I., Petoukhov, M. V., Coda, A., Curti, B., Ravasio, S., Vanoni, M. A., and Mattevi, A. (2003) The Active Conformation of Glutamate Synthase and its Binding to Ferredoxin. *J. Mol. Biol.* 330, 113–128.
- (4) Hirasawa, M., Rubio, L. M., Griffin, J. L., Flores, E., Herrero, A., Li, J., Kim, S.-K., Hurley, J. K., Tollin, G., and Knaff, D. B. (2004) Complex formation between ferredoxin and *Synechococcus* ferredoxin:nitrate oxidoreductase. *Biochim. Biophys. Acta, Bioenerg.* 1608, 155–
- (5) Kim, J. Y., Nakayama, M., Toyota, H., Kurisu, G., and Hase, T. (2016) Structural and mutational studies of an electron transfer complex of maize sulfite reductase and ferredoxin. *J. Biochem.* 160, 101–109.
- (6) Dammeyer, T., Bagby, S. C., Sullivan, M. B., Chisholm, S. W., and Frankenberg-Dinkel, N. (2008) Efficient Phage-Mediated Pigment Biosynthesis in Oceanic Cyanobacteria. *Curr. Biol.* 18, 442–448.
- (7) Sheftel, A. D., Stehling, O., Pierik, A. J., Elsasser, H.-P., Muhlenhoff, U., Webert, H., Hobler, A., Hannemann, F., Bernhardt, R., and Lill, R. (2010) Humans possess two mitochondrial ferredoxins, Fdx1 and Fdx2, with distinct roles in steroidogenesis, heme, and Fe/S cluster biosynthesis. *Proc. Natl. Acad. Sci. U. S. A. 107*, 11775–11780.
- (8) Heinzelman, P., Romero, P. A., and Arnold, F. H. (2013) Efficient Sampling of SCHEMA Chimera Families to Identify Useful Sequence Elements. *Methods Enzymol.* 523, 351–368.

- (9) Silberg, J. J., Endelman, J. B., and Arnold, F. H. (2004) SCHEMA-Guided Protein Recombination. *Methods Enzymol.* 388, 35–42
- (10) Crameri, A., Raillard, S.-A., Bermudez, E., and Stemmer, W. P. C. (1998) DNA shuffling of a family of genes from diverse species accelerates directed evolution. *Nature* 391, 288–291.
- (11) Mateljak, I., Rice, A., Yang, K., Tron, T., and Alcalde, M. (2019) The Generation of Thermostable Fungal Laccase Chimeras by SCHEMA-RASPP Structure-Guided Recombination *in Vivo. ACS Synth. Biol.* 8, 833–843.
- (12) Otey, C. R., Landwehr, M., Endelman, J. B., Hiraga, K., Bloom, J. D., and Arnold, F. H. (2006) Structure-Guided Recombination Creates an Artificial Family of Cytochromes P450. *PLoS Biol. 4*, No. e112.
- (13) Otey, C. R., Silberg, J. J., Voigt, C. A., Endelman, J. B., Bandara, G., and Arnold, F. H. (2004) Functional Evolution and Structural Conservation in Chimeric Cytochromes P450. *Chem. Biol.* 11, 309–318
- (14) Plummer, S. M., Plummer, M. A., Merkel, P. A., Hagen, M., Biddle, J. F., and Waidner, L. A. (2016) Using directed evolution to improve hydrogen production in chimeric hydrogenases from *Clostridia* species. *Enzyme Microb. Technol.* 93–94, 132–141.
- (15) Boehm, M., Alahuhta, M., Mulder, D. W., Peden, E. A., Long, H., Brunecky, R., Lunin, V. V., King, P. W., Ghirardi, M. L., and Dubini, A. (2016) Crystal structure and biochemical characterization of *Chlamydomonas* FDX2 reveal two residues that, when mutated, partially confer FDX2 the redox potential and catalytic properties of FDX1. *Photosynth. Res.* 128, 45–57.
- (16) Gou, P., Hanke, G. T., Kimata-Ariga, Y., Standley, D. M., Kubo, A., Taniguchi, I., Nakamura, H., and Hase, T. (2006) Higher Order Structure Contributes to Specific Differences in Redox Potential and Electron Transfer Efficiency of Root and Leaf Ferredoxins[†]. *Biochemistry* 45, 14389–14396.
- (17) Hase, T., Mizutani, S., and Mukohata, Y. (1991) Expression of Maize Ferredoxin cDNA in *Escherichia coli*: Comparison of Photosynthetic and Nonphotosynthetic Ferredoxin Isoproteins and their Chimeric Molecule. *Plant Physiol.* 97, 1395–1401.
- (18) Hirota, N., Matsuo, T., Ikeda, A., Yatsunami, R., Fukui, T., and Nakamura, S. (2005) Role of an N-terminal domain found in the ferredoxin from extremely halophilic archaeon *Haloarcula japonica*. *J. Jpn. Soc. Extremophiles* 4, 14–24.
- (19) Schmitz, S., Schrautemeier, B., and Böhme, H. (1993) Evidence from directed mutagenesis that positively charged amino acids are necessary for interaction of nitrogenase with the [2Fe-2S) heterocyst ferredoxin (FdxH) from the cyanobacterium *Anabaena* sp. PCC7120. *Mol. Gen. Genet.* 240, 455–460.
- (20) Low, D. W., and Hill, M. G. (2000) Backbone-Engineered High-Potential Iron Proteins: Effects of Active-Site Hydrogen Bonding on Reduction Potential. *J. Am. Chem. Soc.* 122, 11039—11040.
- (21) Kitagawa, Y., Shoji, M., Saito, T., Nakanishi, Y., Koizumi, K., Kawakami, T., Okumura, M., and Yamaguchi, K. (2008) Theoretical studies on effects of hydrogen bonds attaching to cysteine ligands on 4Fe-4S clusters. *Int. J. Quantum Chem.* 108, 2881–2887.
- (22) Niu, S., and Ichiye, T. (2009) Insight into Environmental Effects on Bonding and Redox Properties of [4Fe-4S] Clusters in Proteins. J. Am. Chem. Soc. 131, 5724–5725.
- (23) Atkinson, J. T., Campbell, I. J., Thomas, E. E., Bonitatibus, S. C., Elliott, S. J., Bennett, G. N., and Silberg, J. J. (2019) Metalloprotein switches that display chemical-dependent electron transfer in cells. *Nat. Chem. Biol.* 15, 189–195.
- (24) Campbell, I. J., Olmos, J. L., Xu, W., Kahanda, D., Atkinson, J. T., Sparks, O. N., Miller, M. D., Phillips, G. N., Bennett, G. N., and Silberg, J. J. (2020) *Prochlorococcus* phage ferredoxin: structural characterization and interactions with cyanobacterial sulfite reductases. *J. Biol. Chem.* 295, 10610–10623.
- (25) Nechushtai, R., Lammert, H., Michaeli, D., Eisenberg-Domovich, Y., Zuris, J. A., Luca, M. A., Capraro, D. T., Fish, A., Shimshon, O., Roy, M., Schug, A., Whitford, P. C., Livnah, O.,

- Onuchic, J. N., and Jennings, P. A. (2011) Allostery in the ferredoxin protein motif does not involve a conformational switch. *Proc. Natl. Acad. Sci. U. S. A.* 108, 2240–2245.
- (26) Fish, A., Danieli, T., Ohad, I., Nechushtai, R., and Livnah, O. (2005) Structural Basis for the Thermostability of Ferredoxin from the Cyanobacterium *Mastigocladus laminosus*. *J. Mol. Biol.* 350, 599–608.
- (27) Heinzelman, P., Snow, C. D., Wu, I., Nguyen, C., Villalobos, A., Govindarajan, S., Minshull, J., and Arnold, F. H. (2009) A family of thermostable fungal cellulases created by structure-guided recombination. *Proc. Natl. Acad. Sci. U. S. A. 106*, 5610–5615.
- (28) Bloom, J. D., Labthavikul, S. T., Otey, C. R., and Arnold, F. H. (2006) Protein stability promotes evolvability. *Proc. Natl. Acad. Sci. U. S. A. 103*, 5869–5874.
- (29) Ho, M. L., Adler, B. A., Torre, M. L., Silberg, J. J., and Suh, J. (2013) SCHEMA Computational Design of Virus Capsid Chimeras: Calibrating How Genome Packaging, Protection, and Transduction Correlate with Calculated Structural Disruption. *ACS Synth. Biol.* 2, 724–733.
- (30) Bottin, H., and Lagoutte, B. (1992) Ferrodoxin and flavodoxin from the cyanobacterium *Synechocystis* sp. PCC 6803. *Biochim. Biophys. Acta, Bioenerg.* 1101, 48–56.
- (31) Dutton, J. E., and Rogers, L. J. (1978) Isoelectric focusing of ferredoxins, flavodoxins and a rubredoxin. *Biochim. Biophys. Acta, Protein Struct.* 537, 501–506.
- (32) Böhme, H., and Schrautemeier, B. (1987) Comparative characterization of ferredoxins from heterocysts and vegetative cells of *Anabaena variabilis*. *Biochim. Biophys. Acta, Bioenerg.* 891, 1–7.
- (33) Stephens, P. J., Thomson, A. J., Dunn, J. B. R., Keiderling, T. A., Rawlings, J., Rao, K. K., and Hall, D. O. (1978) Circular dichroism and magnetic circular dichroism of iron-sulfur proteins. *Biochemistry* 17, 4770–4778.
- (34) Ta, D. T., and Vickery, L. E. (1992) Cloning, sequencing, and overexpression of a [2Fe-2S] ferredoxin gene from *Escherichia coli. J. Biol. Chem.* 267, 11120–11125.
- (35) Barstow, B., Agapakis, C. M., Boyle, P. M., Grandl, G., Silver, P. A., and Wintermute, E. H. (2011) A synthetic system links FeFehydrogenases to essential *E. coli* sulfur metabolism. *J. Biol. Eng.* 5, 7.
- (36) Wu, B., Atkinson, J. T., Kahanda, D., Bennett, G. N., and Silberg, J. J. (2020) Combinatorial design of chemical-dependent protein switches for controlling intracellular electron transfer. *AIChE I.* 66, No. e16796.
- (37) Aliverti, A., Faber, R., Finnerty, C. M., Ferioli, C., Pandini, V., Negri, A., Karplus, P. A., and Zanetti, G. (2001) Biochemical and Crystallographic Characterization of Ferredoxin-NADP+ Reductase from Nonphotosynthetic Tissues. *Biochemistry* 40, 14501–14508.
- (38) Hirasawa, M., Nakayama, M., Hase, T., and Knaff, D. B. (2004) Oxidation-reduction properties of maize ferredoxin:sulfite oxidoreductase. *Biochim. Biophys. Acta, Bioenerg.* 1608, 140–148.
- (39) Iwasaki, T., Kappl, R., Bracic, G., Shimizu, N., Ohmori, D., and Kumasaka, T. (2011) ISC-like [2Fe-2S] ferredoxin (FdxB) dimer from Pseudomonas putida JCM 20004: structural and electron-nuclear double resonance characterization. *JBIC, J. Biol. Inorg. Chem.* 16, 923–935.
- (40) Macedo-Ribeiro, S., Martins, B. M., Barbosa Pereira, P., Buse, G., Huber, R., and Soulimane, T. (2001) New insights into the thermostability of bacterial ferredoxins: high-resolution crystal structure of the seven-iron ferredoxin from *Thermus thermophilus*. *JBIC*, *J. Biol. Inorg. Chem.* 6, 663–674.
- (41) Macedo-Ribeiro, S., Darimont, B., and Sterner, R. (1997) Structural features correlated with the extreme thermostability of 1[4Fe-4S] ferredoxin from the hyperthermophilic bacterium *Thermotoga maritima*. *Biol. Chem.* 378, 331–336.
- (42) Meyer, M. M., Silberg, J. J., Voigt, C. A., Endelman, J. B., Mayo, S. L., Wang, Z.-G., and Arnold, F. H. (2003) Library analysis of SCHEMA-guided protein recombination. *Protein Sci.* 12, 1686–1693.
- (43) Meyer, M. M., Hochrein, L., and Arnold, F. H. (2006) Structure-guided SCHEMA recombination of distantly related β -lactamases. *Protein Eng., Des. Sel.* 19, 563–570.

- (44) Leal, S. S., and Gomes, C. M. (2008) On the relative contribution of ionic interactions over iron-sulfur clusters to ferredoxin stability. *Biochim. Biophys. Acta, Proteins Proteomics* 1784, 1596–1600.
- (45) Lei, H., Guo, Y., Hu, X., Hu, C., Hu, X., and Li, H. (2017) Reversible Unfolding and Folding of the Metalloprotein Ferredoxin Revealed by Single-Molecule Atomic Force Microscopy. *J. Am. Chem. Soc.* 139, 1538–1544.
- (46) Botelho, H. M., and Gomes, C. M. (2011) Structural reorganization renders enhanced metalloprotein stability. *Chem. Commun.* 47, 11149.
- (47) Li, Y., Drummond, D. A., Sawayama, A. M., Snow, C. D., Bloom, J. D., and Arnold, F. H. (2007) A diverse family of thermostable cytochrome P450s created by recombination of stabilizing fragments. *Nat. Biotechnol.* 25, 1051–1056.
- (48) Voigt, C. A., Martinez, C., Wang, Z.-G., Mayo, S. L., and Arnold, F. H. (2002) Protein building blocks preserved by recombination. *Nat. Struct. Biol.* 9, 553–558.
- (49) Engler, C., Kandzia, R., and Marillonnet, S. (2008) A One Pot, One Step, Precision Cloning Method with High Throughput Capability. *PLoS One* 3, No. e3647.
- (50) Salis, H. M. (2011) The Ribosome Binding Site Calculator. *Methods Enzymol.* 498, 19–42.
- (51) Edgar, R. C. (2004) MUSCLE: multiple sequence alignment with high accuracy and high throughput. *Nucleic Acids Res.* 32, 1792–1797.
- (52) Waterhouse, A. M., Procter, J. B., Martin, D. M. A., Clamp, M., and Barton, G. J. (2009) Jalview Version 2–a multiple sequence alignment editor and analysis workbench. *Bioinformatics* 25, 1189–1191.
- (53) Artimo, P., Jonnalagedda, M., Arnold, K., Baratin, D., Csardi, G., de Castro, E., Duvaud, S., Flegel, V., Fortier, A., Gasteiger, E., Grosdidier, A., Hernandez, C., Ioannidis, V., Kuznetsov, D., Liechti, R., Moretti, S., Mostaguir, K., Redaschi, N., Rossier, G., Xenarios, I., and Stockinger, H. (2012) ExPASy: SIB bioinformatics resource portal. *Nucleic Acids Res.* 40, W597–W603.
- (54) Schrödinger, LLC. (2015) PyMOL Molecular Graphics System, Version 1.8.
- (55) Li, B., and Elliott, S. J. (2016) The Catalytic Bias of 2-Oxoacid:ferredoxin Oxidoreductase in CO_2 : evolution and reduction through a ferredoxin-mediated electrocatalytic assay. *Electrochim. Acta* 199, 349–356.
- (56) Mutter, A. C., Tyryshkin, A. M., Campbell, I. J., Poudel, S., Bennett, G. N., Silberg, J. J., Nanda, V., and Falkowski, P. G. (2019) De novo design of symmetric ferredoxins that shuttle electrons *in vivo*. *Proc. Natl. Acad. Sci. U. S. A. 116*, 14557–14562.
- (57) Oliphant, T. E. (2007) Python for Scientific Computing. Comput. Sci. Eng. 9, 10-20.